CONCRETE LIBRARY OF JSCE NO. 36, DECEMBER 2000

# THREE-DIMENSIONAL MODELLING OF REINFORCED CONCRETE WITH MULTI-DIRECTIONAL CRACKING

(Re-editing from Proceedings of JSCE, V-45, No.634, pp.349-368, 1999.11)

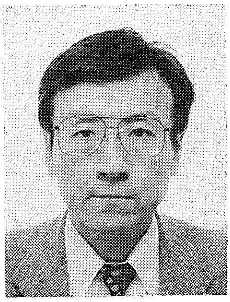

Bernhard HAUKE

Koichi MAEKAWA

This paper presents a three-dimensional (3D) constitutive model for non-linear finite element (FE) analysis of reinforced concrete with special attention to cracked concrete. Post-cracking formulations derived from uni-axial tension are generalized into spatially arbitrarily inclined cracks in multiple directions. Anisotropic concrete tension fracturing and reinforcement mean yield levels of the spatially averaged RC model in association with a 3D RC-zoning concept are discussed. The proposed model is verified by numerically simulating inherently 3D shear failure of RC members subjected to torsion and RC short columns loaded in multi-directional shear.

***Key Words:*** *Multi-directional crack, 3D-constitutive law, anisotropic fracture, finite element analysis, zoning, shear failure*

Bernhard Hauke obtained his Dipl.-Ing. from Darmstadt University of Technology, Germany in 1995 and Ph. D. from the University of Tokyo in 1998. His research interests relate to three-dimensional RC analysis of high nonlinearity and numerical simulation of concrete damage and fracture. At present, he serves as a structural engineer in HOCHTIEF IKS, Bockenheimer Landstr, Frankfurt, Germany.

Koichi Maekawa is a professor in the Department of Civil Engineering at The University of Tokyo. He earned his D.Eng. from the University of Tokyo in 1985. The structural mechanics and constitutive laws for reinforced concrete have been investigated as his academic major background. He joined the project for development of self-compacting concrete in 1985-1989 with his colleagues. After innovation of the first prototype of the super-fluidized concrete, Dr. Maekawa has been engaged in the DuCOM project for concrete composite microstructure development and computational durability assessment.

## 1. INTRODUCTION

With continuing computer hardware development and with new findings in materials research, the finite element method is finding application in the simulation of experiments and the prediction of structural safety and serviceability of reinforced concrete in general. Almost three decades of worldwide research effort have led to the development of elaborate constitutive models of reinforced concrete for in-plane structures. At the same time, only a few applications involving full 3D modeling of structural geometry, stress states, and loading patterns have emerged in the literature.

In this paper, 3D constitutive models of reinforced concrete with special attention to post cracking formulations are introduced. In 2D-reduced analysis, element-wise quasi-isotropic cracked reinforced concrete formulations may be reasonable to some extent since crack orientation can only be directed in the plane. In the more generic approach of full 3D, however, stress and strain fields are modeled as is, and anisotropy of the spatially averaged RC-model is encountered. This is because cracks with any discretionary inclination are allowed in the 3D space whilst the full bonding effect can be assumed only in the direction(s) of reinforcing bar(s). Consequently, the post-cracking response based on the smeared modeling concept, derived from uni-axial tension, must be extended to the more generic situation of spatially arbitrary crack inclinations with respect to the reinforcement, as may be encountered in reinforced concrete subjected to non-trivial loading.

For verification of the proposed 3D constitutive relations, plain and reinforced concrete members in torsion and short RC columns under multi-lateral loading in shear were selected for experiments. The load-bearing mechanism becomes inherently three-dimensional in these cases, and the problem cannot be solved by 2D analysis. In fact, most reinforced concrete structures are subjected to complex loading patterns over their lifetimes. Short columns serving highway bridges, for example, are exposed to axial loading and combined uni-axial shear and flexure under service conditions, and this is a standard 2D problem. However, in the case of earthquake or accidental impact, such columns have to sustain multi-directional shear and/or torsion. As a result, it is necessary not only to understand but also to numerically simulate the complex behavior of RC structures under non-proportional multi-lateral loading patterns (see **Fig.1**). In part, this is to meet the needs of the performance-based design philosophy of next-generation structural codes, which require engineers to check specified limit states and guarantee quality to the public. Here, especially, structures have to be checked for seismic or accidental loading in reasonable consistency with material and structural mechanics, and a versatile computational tool that can examine structural performance is required.

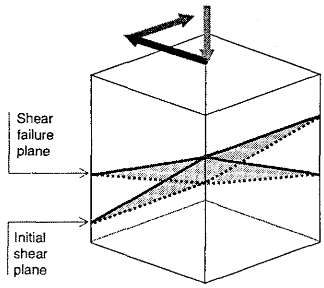


**Fig.1** Short RC-column subjected to non-proportional multi-directional

## 2. RC-BRICK ELEMENTS

### 2.1 General concept

Reinforced concrete is idealized as a composite material consisting of concrete with reinforcement superimposed on it. By combining the constitutive laws of average stress and average strain for concrete and reinforcement[1], respectively, an RC brick element has been constructed. In the FE computations, isoparametric brick elements with 20 nodes are used for reinforced concrete. Concrete is, according to its state, Computed by routines for un-cracked or cracked concrete in the structural analysis frame (see **Fig.2**). The generation of cracks is the branch point into strong anisotropic nonlinearity and, at the same time, it marks the switch in concrete models according the proposed analysis concept. Crack initiation is determined by a simple Rankine criterion. Realizing that damage accumulation in concrete subjected to compression and tension prior to cracking is basically of a blunt non-local continuum nature, while post-cracking behavior can be thought of as a highly localized process, the separate treatment of un-cracked and cracked concrete seems to be reasonable. The phenomenon of post-peak compression softening remains un-addressed and external to the present framework; it forms a challenging topic of further research.

## 2.2 Extended elasto-plastic and continuum fracture model for un-cracked concrete

In the pre-cracking range, the triaxial elasto-plastic and continuum damage/fracturing (EPF) model for concrete[2)] is employed. The mechanical behavior of the concrete is idealized as combined plasticity and continuum fracturing, which identify induced permanent deformations and the loss of elastic energy absorption capacity, respectively. The model, which was originally developed for full triaxial compression, has recently been extended to the whole of 3D-space, covering the tension domain of pre-cracked concrete[3)] as shown in **Fig.2**.

## 2.3 3D multi-directional smeared crack model

The introduction of cracks in concrete marks the transition from an idealised 3D continuum, as treated by the EPF-model, into a highly anisotropic medium. Owing to crack stress release, the 3D-confinement effect may be assumed to be much reduced for cracked concrete. Noting this inherent breakdown of 3D continuity, the smeared crack model in of three dimensions based on a cracked concrete in-plane constitutive law under cyclic forces was been proposed by Maekawa et al.[4)]. After closure of pre-cracking under load reversals, the constitutive model is switched back to the elasto-plastic and continuum fracture model of un-cracked concrete, and the tri-axial confinement effect on concrete in compression is considered again.

An orthogonal Cartesian co-ordinate system is assumed, whose principal axis (1) is normal to the initially introduced crack plane and the remaining axes (2 and 3) are placed within the first crack reference plane. Here, we can define two-dimensional sub-spaces designated by axes (1, 2), (2, 3), and (1, 3) as shown in **Fig.3**. The initial crack would be contained in the (1, 2) and (1, 3) planes, while plane (2, 3) coincides with the plane of the initial crack. Any further crack would then be completely within the fixed two-dimensional sub-spaces determined by the initial crack.

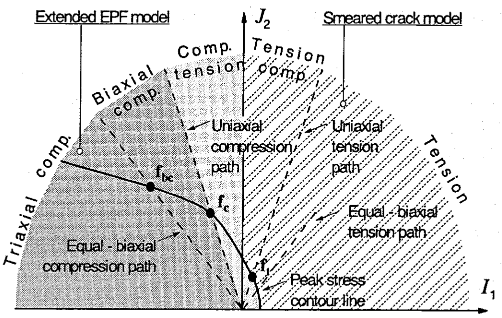


**Fig.2** Generic concrete models for complete

Now, the partial stresses rooted in the crack projection on (i, j) can be computed by using the in-plane RC constitutive law accompanying multi-directional cracking. Let $\sigma_{ij}^{(k,l)}$ denote the reduced component stress computed from mean strain on the (k, l) sub-space. When we simply assume the total load carrying mechanism as being composed of partial stresses in the three sub-spaces, we have,

$$\sigma_{ii} = \frac{1}{2}\sum_{k \neq i} \sigma_{ii}^{(i,k)} \quad \left(\varepsilon_{st} \,|_{s,t=i \vee k}\right) \qquad (1a)$$

$$\sigma_{ij} \,|_{i \neq j} = \sigma_{ij}^{(i,j)} \quad \left(\varepsilon_{st} \,|_{s,t=i \vee k}\right) \qquad (1b)$$

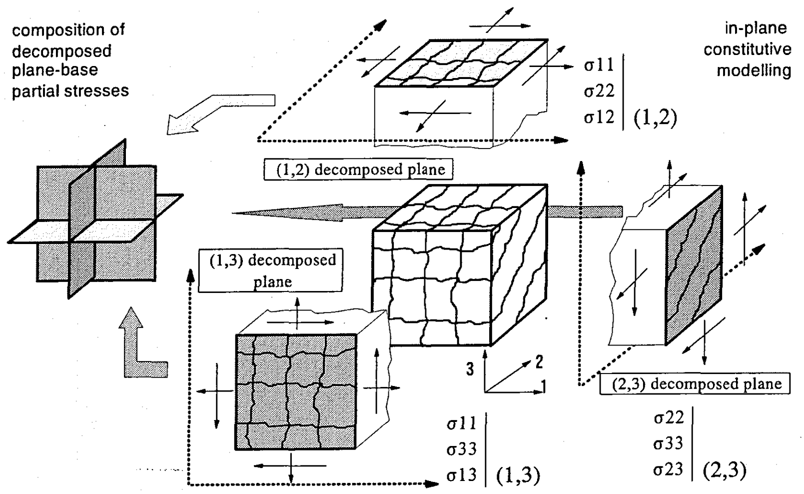


**Fig.3** Re-composition of load carrying mechanism of 3D cracked concrete solids with multi-directional cracking

where the in-plane membrane constitutive equation is used to compute component stress $\sigma_{ij}^{(k,l)}$ from sub-space strains as $\varepsilon_{st(s,t \vee k,l)}$.

For computation of 2D sub-space component stresses, the newly proposed four-way fixed crack model of Fukuura and Maekawa[5] is utilised. The model considers up to nine fictitious cracks at each integration point in the scheme of 3D smeared crack idealisation. The in-plane smeared crack model is composed of a tension stiffening model across cracks, a compression stiffening/softening model parallel to cracks, and shear transfer model along cracks, as described in Okamura and Maekawa[1]. The scheme of the four-way fixed crack model, as well as the management of active and dormant cracks and their verifications, are given in the literature by Fukuura and Maekawa[5].

### 2.4 Distributed reinforcement

In the three-dimensional modeling of RC-structures, modeling of smeared and distributed reinforcing bars in space is thought to offer advantages, over detailed structural modeling since it does not require any additional nodes or elements as would be necessary for discrete or embedded representations. Hence, it simplifies the generation of 3D reinforced concrete meshes. Furthermore, if a discrete reinforcing bar model were to be chosen, much finer finite elements would have to be allocated to numerically simulate localized yielding of reinforcement close to crack planes.

In contrast, the smeared reinforcement model can take into account the localized plasticity in a finite element by adapting a spatially averaged constitutive law of steel embedded in concrete with bond interaction. Then, for reinforcement orthogonally arranged in space, numerical representation without dowel shear stiffness had been adopted. In the smeared approach, localization of initial steel plasticity close to cracks and local bond slip effects are considered in computing the mean stress-strain relation based on the local bond-slip-strain behaviour[1].

## 3. SPATIALLY ANISOTROPIC POST-CRACKING RESPONSE

### 3.1 Effective embedment (RC) zone

In 3D finite element computations of actual scale reinforced concrete structures, the number of finite elements is limited due to restricted computational power. For engineering purposes, larger elements are likely to be employed. Within the volume of the finite element domain, both primary and secondary cracks may develop (**Fig.4**), whilst concrete between cracks can still sustain tensile stresses transferred through bond action from the reinforcement. Hence, spatially average stress – average strain relations[1] representing the mean behaviour of the element volume have been developed and are widely used.

If we could allocate many smaller elements, such that all local cracks as well as un-cracked concrete between primary cracks could be separately identified, no average-based concrete and reinforcement models would be necessary. In such a case, of course, no tension stiffening or RC-zoning needs to be considered, since the contribution of concrete between cracks is intrinsically considered.

However, as noted above, such a fine FE mesh cannot be analysed for RC structures of engineering interest within reasonable time considering available computer technology. Thus, for 3D finite elements of some finite volume, a so-called zoning concept [8] is necessary to correctly handle distinct average constitutive laws of concrete to close to and far from reinforcement and to consider spatial orientations of the bonding effect on concrete.

As a matter of fact, bonding is an inherently 3D problem given the conical shape of secondary cracking (**Fig.4**), which cannot be treated physically consistently in the 2D realm. Strictly speaking, any 2D approach[6] that omits tension stiffening formulations and uses a large number of small elements instead is inconsistent. In that case, secondary bond cracks, once generated, can propagate progressively since the crack front is just a point. In reality, secondary bond cracks may propagate in a conical shape and the circular crack front enlarges as the crack ligament develops. Here, cracking cannot be progressive; rather because of the enlarging crack front, propagation eventually comes to a half.

The tension stiffening model for reinforced concrete, as mentioned in the previous section as an essential part of the average-based cracked concrete routine, was derived from uni-axial tension tests [7]. In these tests, tensile strain was nearly uniformly distributed over the section and the reinforcement ratio was above the minimum one. In this case, cracks form only normal to the reinforcement and the softening behavior of the concrete volume as a whole is controlled by the reinforcement. In actual reinforced concrete structures, however, strain gradients and reinforcement ratios below the critical level may be found, and cracks may not always form normal to the reinforcing bars. Consequently, concrete close to the reinforcement may, due to the bonding effect, stiffen in a similar way as observed in the uni-axial tension tests, while concrete far away from the reinforcement behaves as brittle plain concrete[8].

Gupta and Tanabe[9] raised the question of whether tension-stiffening diagrams obtained from uni-axial tension tests could be applied to the general loading of RC structures exhibiting strain gradients. Barzegar and Maddipudi[10] presented a solution for this problem by selecting distinct fracture energies for different plain and reinforced concrete structures, which might reflect the average behavior of the structure. For an un-reinforced specimen, the specified fracture energy is in the common range of concrete. For reinforced concrete members, on the other

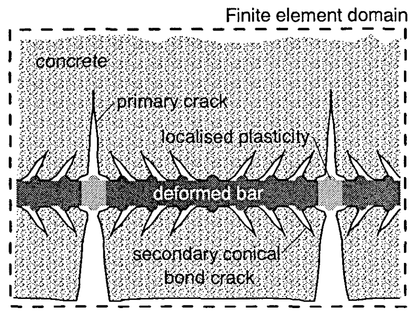


**Fig.4** Formation of cracks in finite element

hand, an isotropic tension stiffening effect is implicitly considered by allocating larger fracture energy values. Then, depending on the reinforcement arrangement and the expected strain gradient, a kind of fracture energy could be decided, which would be a structural rather than a material property. However, no information is given ash how the fracture energy would be determined for different RC structures or whether it can be clearly determined or is just a mere fitting parameter.

The above discussion makes clear that some sort of more rational method is desirable. This would allow us to determine the volume of concrete to which bonding extends, for which softening behavior is controlled by the reinforcement through bond action and which must be distinguished from plain concrete because of its evident tension stiffening characteristics. Such a zone might be called the effective embedment or RCzone[8]. A simple engineering method of determining the RC zone in 2D problems based on a single-bar equilibrium condition as shown in **Fig.5** has been proposed by An et al.[8]. The RC zone for a single reinforcing bar is determined from the condition that the tensile force carried by the RC zone concrete just prior to cracking must be equal to the yield force which the reinforcing bar can support at maximum through the bond mechanism after cracking. This is formulated as[8]

$$A_{RC} = \frac{A_{st} \cdot f_y}{f_t} \qquad (2)$$

where, $A_{RC}$ is the maximum area of the bond effect zone in concrete, $A_{st}$ is the area of the steel bar, $f_t$ is concrete tensile strength, and $f_y$ is yielding strength of the steel bar (**Fig.5**). Or, in other words, the reinforcement ratio of the RC zone is assumed equal to the critical reinforcement ratio, $f_t/f_y$. Overlapping RC zones associated with neighboring reinforcing bars are not additionally accounted for, and neither are parts of the RC zone that fall outside the structure boundary, as illustrated in **Fig.5**.

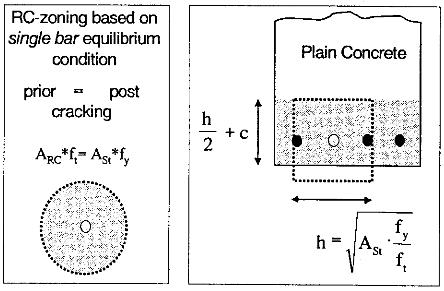


**Fig.5** Single bar RC zoning concept

As originally proposed, this 2D RC-zoning method[8] does not account for the directional features of the bond effect on concrete. Finite elements found to be within the effective embedment zone of a reinforcing bar are designated as isotropic tension stiffening. For a simple arrangement of reinforcement and a load pattern that chiefly generates cracks perpendicular to the reinforcement, this assumption may lead to good results.

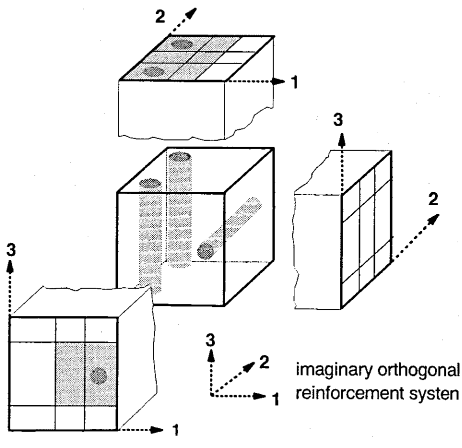


**Fig.6** 3D RC zoning concept using an imaginary orthogonal reinforcing system

To overcome this restriction by adapting a more versatile RC-zoning concept, an imaginary three-directional, orthogonal reinforcement system is introduced. In each of the respective directions, the RC-zoning method is applied independently. Then, if none of those three directions of a control volume contains reinforcement, isotropic plain concrete is assumed, while all three directions containing reinforcement would represent isotropic reinforced concrete. Any other combination, however, would lead to an anisotropic reinforced/plain concrete behavior of the respective finite elements in the control volume (**Fig.6**).

It had been found that for deep structural members, such as beams or columns, the influence of splitting cracks on bonding and tension stiffening is negligible, even if the concrete cover is deficient on one side[11]. This is because of the confinement of the surrounding concrete and possible hoop reinforcement[11]. Consequently, in this study, no reduction of the RC zone to account for insufficient concrete cover is made for simplicity.

### 3.2 Anisotropic tension fracture

The post cracking concrete tension model was proposed by Okamura and Maekawa[1] as

$$\sigma_t = f_t(\varepsilon_{tu}/\varepsilon_t)^c \qquad (3)$$

where "c" is a parameter describing the inclination of the descending envelope curve and $\varepsilon_{tu}$ is the cracking strain (see **Fig.7**).

For plain concrete softening, in order to avoid spurious mesh dependence, the softening parameter in Eq.(3) has to be defined by means of an energy, based fracture mechanics requirement[8]. According to the crack band theory[12], plain concrete softening can be determined from the fracture energy in association with the reference length of smeared crack elements (**Fig.8**). In the present post-cracking tension model, the softening parameter denoted by "$c$" is obtained by satisfying

$$\int \sigma_t d\varepsilon_t = G_f / l_r \qquad (4)$$

where, $G_f$; $l_r$ are the fracture energy of concrete and the reference length on which the average softening stress-strain relation is defined. Simple a priori methods for determining $l_r$ using the square root of element area[8] or volume are, strictly speaking, restricted to regular meshes with cracks running mostly parallel to the mesh peripheral lines.

However, for the general case of rectangular solid elements with inclined cracks, a more precise estimation seems desirable. In this research, tension softening is determined in each global direction, respectively, by taking the corresponding element dimension as the reference length (**Fig.8**). For cracks not running parallel to one of the element faces, an interpolation scheme based on normalized fracture energy $G_f^*$ is described in the following section.

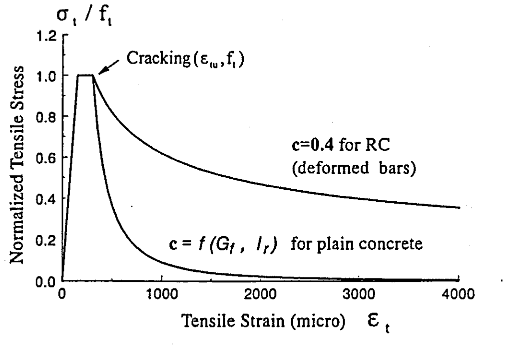


**Fig.7** Tension model for plain and reinforced concrete[1]

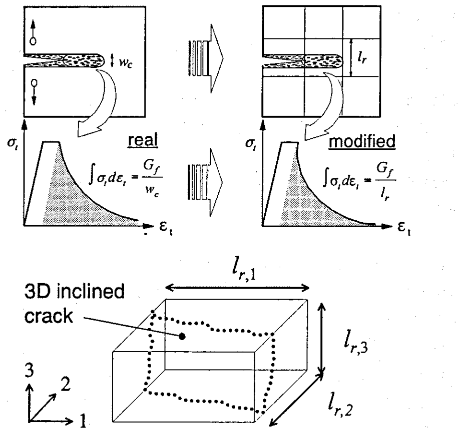


**Fig.8** Crack band theory for smeared modeling of concrete tension fracture in 2D and 3D

The tension stiffness model for reinforced concrete has the same mathematical form as the softening model[1]. In the case of RC, softening factor c in Eq.(3) has been verified as constant (0.4 for deformed bars) and independent of finite element size, provided that the reinforcement ratio of the volume concerned is higher than the critical reinforcement ratio[1]. With respect to the RC-zoning method previously described, this condition is always fulfilled.

The different softening/stiffening behaviour of plain and reinforced concrete and the zoning method have been introduced in general. Now, their interaction in 3D applications will be discussed. A crack generated in a concrete control volume may have any arbitrary inclination in space. If such a crack is located in the plain concrete zone, the softening behaviour differs with crack orientation and element geometry. For a control volume containing reinforcement in one or several directions the average softening/stiffening behaviour depends furthermore on the crack inclination relative to the bar. A cracked concrete normal to the reinforcement will exhibit stiffening due to bond development while another parallel crack without any intersection with the steel would see softening. Consequently, a crack which is neither parallel nor normal to a reinforcing bar but arbitrarily inclined must result in mixed softening/stiffening behavior, as shown in **Fig.9**. It might be opportune to call this dependency of reinforced concrete post-cracking behaviour on crack orientation with respect to reinforcement "anisotropic softening".

Firstly, applying RC zoning in all three directions of the reinforcement system defines distinct softening and stiffening characteristics in an orthogonal system. For randomly inclined cracks, the softening behavior must be interpolated. Since the relationship between the softening parameter and fracture energy is highly nonlinear, parameter "c" cannot be extracted by mere interpolation. Non-dimensional fracture energy, normalized by tension strength and reference length, can be used instead. It is defined as

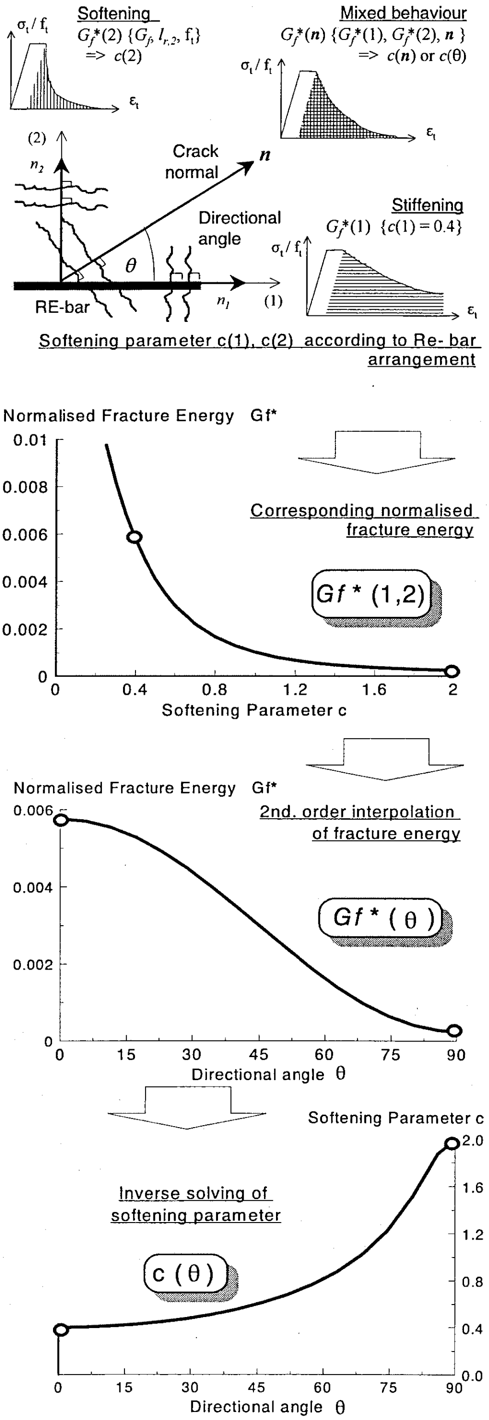


**Fig.9** Fracture energy-based interpolation scheme of softening parameter for inclined cracks

$$G_f^* = \frac{G_f}{f_t l_r} = \frac{1}{f_t}\int_{\varepsilon_{tu}}^{\varepsilon_{te}} \sigma_t d\varepsilon_t + \frac{1}{4}\varepsilon_{tu} \quad (5)$$

By substituting Eq.(3) into Eq.(5) and executing the integration, we have

$$G_f^* = \frac{\varepsilon_{tu}}{c-1}\left[1-\left(\frac{\varepsilon_{te}}{\varepsilon_{tu}}\right)^{1-C}\right] + \frac{1}{4}\varepsilon_{tu} \quad (6)$$

where, $\varepsilon_{te}$ denotes the ultimate tensile strain used as the integration limit. Then, $G_f^*$ for plain concrete can be computed based on fracture mechanical requirement Eq.(5) and for reinforced concrete based on the empirical stiffening parameter in Eq.(6).

Here, the normalized fracture energy defined in the orthogonal system has to be interpolated. As a slight deviation of the crack from the bar direction would not cause much reduction of fracture energy, a $2^{nd}$ order interpolation is proposed as a simple mechanical model. An in-plane simplified situation as illustrated in **Fig.9** would lead to

$$G_f^*(n) = \frac{n_1^2 G_f^*(1) + n_2^2 G_f^*(2)}{n_1^2 + n_2^2} \quad (7)$$

where, $n_1$ and $n_2$ are the components of the crack normal unit vector $\boldsymbol{n}$. If we introduce the directional angle $\theta$ of the crack normal relative to the reinforcing bar, these components are $n_1 = \cos\theta$ and $n_2 = \sin\theta$ and hence, we can write the interpolation as

$$G_f^*(\theta) = \cos^2\theta\ G_f^*(1) + \sin^2\theta\ G_f^*(2) \quad (8)$$

Having computed $G_f^*(\theta)$, the softening parameter "c" for an arbitrary angle can be obtained by inversely solving Eq.(6), as shown in **Fig.9**. The conforming 3D interpolation is straightforwardly obtained as

$$G_f^*(n) = \frac{n_1^2 G_f^*(1) + n_2^2 G_f^*(2) + n_3^2 G_f^*(3)}{n_1^2 + n_2^2 + n_3^2} \quad (9)$$

Distinct tension softening and stiffening characteristics in full 3D space are defined and the respective information is transferred to the 2D sub-spaces [4)] where the softening parameter is finally utilised in Eq.(3) for post-cracking tension analysis[1)].

### 3.3 Anisotropic shear transfer model

Since the generation of cracks in concrete is determined by the maximum principal stress criterion, shear stress and strains are zero on the crack plane normal to the maximum principal stress direction at the moment of cracking. However, as loading proceeds, the principal axes of stress and strain rotate, and this eventually leads to the introduction of a new crack. At the same time, the original crack is subjected to shear strain, since it is no longer normal to the principal direction. Then, with the concept of the fixed crack approach, shear transfer along the cracks must be addressed[1)].

The shear model of cracked concrete used in this study is based on the simplified contact density model[13)] in which the rough crack surface is idealized as a large set of contact units with various inclinations and distributed according to a contact density function. In each direction, a contact unit transfers normal and shear stresses, which are formulated by a rigid-plastic model.

The infinite plastic deformation of contact units is in fact imaginary. Bujadham et al.[14)] reported that softening of the shear transfer mechanism was a function of shear displacement along cracks and introduced a degradation component for use in computing the contact stress. A simple shear softening concept that adjusts the contact density shear transfer model for FE computations was been proposed by An et al.[8)]. This involves multiplying the original integral-formed shear transfer model by a decay function (**Fig.10**) as

$$\begin{aligned} \tau &= (G \times \gamma)1.0 && if \quad \gamma < \gamma_u \\ \tau &= (G \times \gamma)(\gamma_u/\gamma)^c && if \quad \gamma \geq \gamma_u \end{aligned} \tag{10}$$

where, $\tau$ is the mean shear stress, $\gamma$ is the mean shear strain, G is the shear secant modulus according to the contact density model[13], $\gamma_u$ is the ultimate shear strain at which softening initiates[8], and $c$ is the softening parameter. The ultimate shear strain was adjusted to 400 μ for plain concrete and, 4000 μ for reinforced concrete[8] and the softening parameter is, for simplicity and lack of other information, assumed to be the same as used for tension softening/stiffening[8]. It has been shown that the shear failure mechanism of RC beams and columns can be numerically simulated for 2D problems[8] if the distinct tension/shear softening as stated above is applied to the reinforced and plain concrete zones, respectively.

In the formulation of the shear decay term in Eq.(10), the slope of the descending branch is altered according to Mode II fracture energy[8]. In interaction with the softening parameter interpolation scheme for anisotropic tension fracturing, the assumed softening branch of the shear transfer model is consistently defined for cracks at arbitrary inclinations with respect to the reinforcing bars.

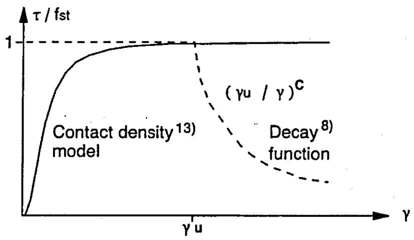


**Fig.10** Original shear transfer (contact density)

On the contrary, the onset of shear transfer decay denoted by $\gamma_u$ needs to be defined for the intermediate case between plain and reinforced concrete. We propose varying the onset of shear transfer decay $\gamma_u$ (ultimate shear strain) depending on the crack inclination in space relative to the reinforcing bars (**Fig.11**) in a similar manner as used for the tension softening parameter. In the orthogonal reinforcement bar system, $\gamma_u$ can be indicated for directions (1), (2), and (3) according to RC zoning and for the arbitrary crack angle, $\gamma_u$ is interpolated as,

$$\gamma_u(n) = \frac{n_1^2\gamma_u(1) + n_2^2\gamma_u(2) + n_3^2\gamma_u(3)}{n_1^2 + n_2^2 + n_3^2} \tag{11}$$

where $n_1$, $n_2$, and $n_3$ are the components of the crack normal unit vector $\boldsymbol{n}$. An in-plane simplified situation is depicted in **Fig.11** and **Fig.12**.

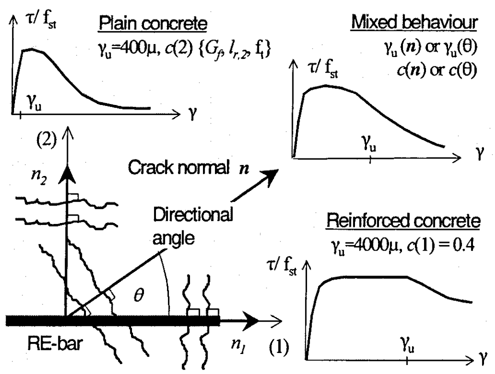


**Fig.11** Anisotropy of shear transfer softening in 2D

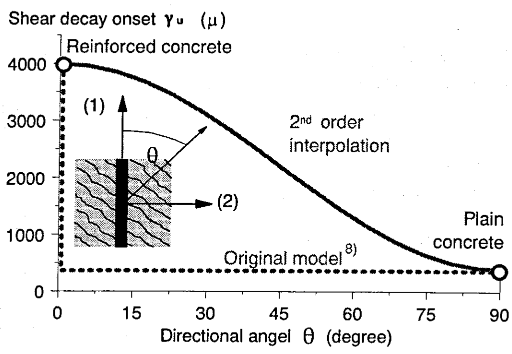


**Fig.12** Interpolation of shear decay onset $\gamma_u$

### 3.4 Anisotropic embedded reinforcement model

A constitutive law for reinforcing bars in concrete has to be numerically modelled based both on the properties of the bare bars and on their bonding effect to concrete[1]. For reinforcing steel, compressive strains are usually significantly smaller than tensile strains, preventing reinforcement from excessive yielding in compression before spalling of concrete cover has occurred. On the tension side, however, highly localised plasticity in the vicinity of cracks has to be taken into account[1]. Consequently, the modelling of reinforcement behaviour in compression and in tension may be different[15]. In compression, complete strain compatibility can be assumed, such that the average behaviour and local behaviour of the reinforcing steel coincide, and a simple bi-linear approximation of bare-bar behaviour suffices. For tensioned reinforcement, on the other hand, to include the effect of localised steel plasticity and bonding within the concept of smeared modelling, an average stress–average strain formulation different from local bare-bar behaviour must be used[1]. An essential input parameter for computing the average response of reinforcement is the effective reinforcement ratio, which is defined as

$$\rho_{eff} = A_{St}/A_{RC} \qquad (12)$$

where, $A_{St}$ is the area of steel considered to be effectively bonded to concrete in tension and $A_{RC}$ is the area of the effective embedment (RC) zone of the concrete where the reinforcing bars can influence crack width (see **Fig.5**). With respect to reinforcement behaviour, $\rho_{eff}$ describes the concrete area relative to the bar size which is effective in restraining free elongation of the steel bar (RC-zone). The larger the effective concrete area (or the smaller $\rho_{eff}$) is, the lower the average yield level will be. For direct tension, the average yield stress of reinforcement embedded in concrete may be computed as[16]

$$\bar{f}_y = f_y - \frac{f_t}{2\rho_{eff}} \qquad (13)$$

After a lower apparent yield stress is defined, a higher average hardening modulus often determines the average stress-strain diagram for tensile reinforcement embedded in the concrete. For the analysis of the most common reinforced concrete structures, such a bi-linear assumption[1] is sufficient since high tensile strains are not encountered due to early concrete compression failure.

However, in seismic analysis or for steel-encased RC-structures, the strain may reach very high tensile values leading eventually to a rupture of the tensile reinforcement. In such a case, bi-linear model would be quite a crude approximation, and may lead to less accurate results. Thus, the versatile computational model for tensile reinforcement proposed by Salem and Maekawa[16] is implemented as a quattro-linear approximation of the average stress-strain law up to failure point (**Fig. 13**).

Experimental work and subsequent mathematical modelling of the average response of steel bars embedded in concrete has been focusing on pure tension with cracks normal to the reinforcement[7),16]. In a more generic situation, however, cracks cannot be expected to always form normal to a steel reinforcing bar. Consequently, formulations derived for direct tension must be revised for application to 2D and 3D computations with arbitrary crack inclination relative to the reinforcing bars.

In **Fig.14,** a simplified 2D situation is depicted. As cracks form normal to the reinforcing bar, the average steel behaviour can be computed according to models derived from direct tension, e.g. Eq.(13), where the effective reinforcement ratio is obtained from the RC zone. If, however, cracks are parallel to the reinforcement, a considerable concrete volume that otherwise could restrain the free elongation of the steel bar may be cut off. In this situation, bare bar behaviour is assumed for simplicity, although some small concrete volume may still be attached to the steel. For any other situation with arbitrarily inclined cracks, the steel response must be between bare-bar and direct tension, as simply illustrated in **Fig.14**.

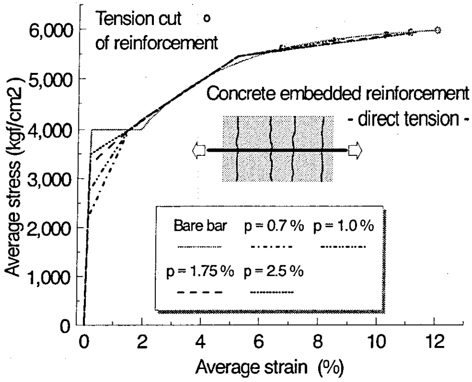


**Fig.13** Quattro-linear average-based tension reinforcement

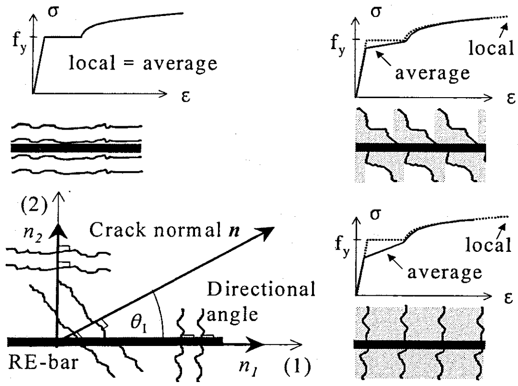


**Fig.14** Anisotropic yield strength of tension reinforcement model[16)]

**Table 1** Material parameters

| | $f_c$' kgf/cm$^2$ | $f_t$ kgf/cm$^2$ | $f_y$ kgf/cm$^2$ | $\rho_{eff}$ % | $\bar{f}_y$ kgf/cm$^2$ | Lc cm |
|---|---|---|---|---|---|---|
| VQ1 | 195 | 11.7 | 4560 | 0.55 | 3511 | 10.0 |
| VQ4 | 175 | 10.9 | 4560 | 1.10 | 4058 | 8.5 |

To consider the varying mean yield strength of steel bars embedded in concrete with respect to crack direction, a 2$^{nd}$ order interpolation between bare-bar ($f_y$) and embedded-bar direct tension ($\bar{f}_y$) behavior is introduced (see **Fig.16**). In each respective reinforcing direction ($i$), the effective mean yield strength $\bar{f}_{y,eff}$ may be computed with respect to crack direction as

$$\bar{f}_{y,eff}(i) = f_y(i) - \left[f_y(i) - \bar{f}_y(i)\right] n_i^2 \qquad (14)$$

where $n_i$ is the component of the crack normal unit vector $\boldsymbol{n}$ in the bar direction ($i$), and $\bar{f}_y(i)$ is the mean yield strength of a reinforcing bar ($i$) if normal cracks are assumed. Introducing the orientation $\theta_i$ of the crack normal $\boldsymbol{n}$ relative to the reinforcing bar ($i$) (**Fig.14**), we have $n_i = \cos\theta_i$ and hence can also write

$$\bar{f}_{y,eff}(i) = f_y(i) - \left[f_y(i) - \bar{f}_y(i)\right] \cos^2\theta_i \qquad (15)$$

To materialise the above-introduced interpolation scheme for effective mean yield level, two reinforced concrete beams subjected to pure torsion are chosen[17)] (**Fig.15, Table 1**). In the case of torsion, cracks would form at an inclination of about 45° to the reinforcing bars, ensuring a situation different from uni-axial tension. In **Fig.16**, the 2$^{nd}$ order interpolation for specimens VQ1 and VQ4 between direct-embedded bar behaviour in tension and bare bar behaviour is shown. In the original test report, the crack pattern is given and the average crack spacing can be estimated (**Table 1**). The average crack spacing can also be computed according to the local bond based semi-empirical model by Salem[18)] as

$$L_c = L_{c0} K_\rho K_y K_t K_c K_d \qquad (16a)$$

$$K_\rho = \left(\rho_{eff}/0.01\right)^{-0.5} \qquad (16b)$$

where, $L_{c0}$ = 50cm. The coefficients describe the influence of effective reinforcement ratio, steel yield strength, concrete tensile and compression strength as well as bar diameter on average crack spacing. Since the average crack spacing is known, Eq.(16) can be re-arranged as

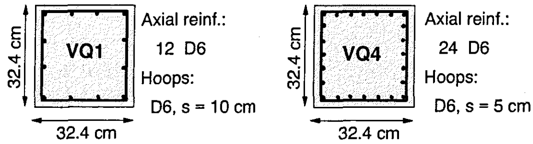


**Fig.15** Torsion beams, Leonhardt and Schelling[17)]

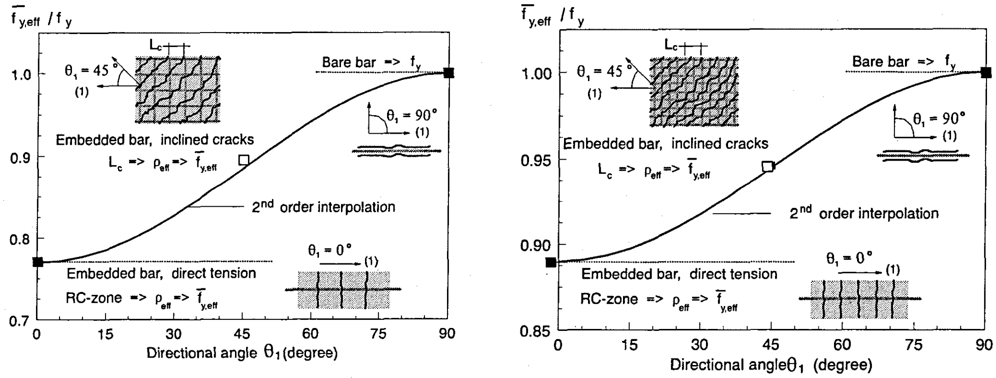


**Fig.16** Comparison of 2nd order interpolation of $\bar{f}_{y,eff}$ with analytical results obtained from observed crack spacing: VQ1 &VQ4[17)]

$$\rho_{eff} = 0.01\left(\frac{L_{c0}K_yK_tK_cK_d}{L_c}\right)^2 \qquad (17)$$

and the effective reinforcement ratio is inversely computed according to the observed average crack spacing. Finally, the apparent mean yield level is obtained from Eq.(13) and plotted over the observed directional angle of $\theta_1 \approx 45°$, as shown in **Fig.16**. Fair agreement with the proposed 2nd order interpolation of mean yield strength, as assumed in Eq.(14), is observed, implicitly verifying the proposed crack direction dependent interpolation of mean yield strength. As an explicit verification, the effectiveness of Eq.(14) in finite element computations will be demonstrated in the next section.

## 4. RCMEMBERS SUBJECTED TO TORSION

Among the basic load bearing mechanisms of structures, namely axial loading, flexure, shear, and torsion, only the latter is a truly three-dimensional problem. All the other basic mechanisms are problems of two dimensions or even only one. For reinforced concrete structures, the case of pure torsion is rather exceptional; torsion commonly acts in combination with other shear and/or bending mechanisms. However, the pure torsion case as a pre-requisite for the general solution of complex loading has been the target of many researchers[17),19),20)]. Since torsion of structural concrete has been experimentally well investigated, it also makes a good analytical target for improving and verifying the 3D analysis concept. After passing the "torsion test", the numerical tool coded as COM3 can be expected to be a step closer to the goal predicting reinforced concrete response under arbitrary load conditions, which is the true and final goal of full 3D reinforced concrete modelling.

### 4.1 Mesh size sensitivity

To verify the general analytical frame and mesh objectivity in inclined cracking situations, free from the effects of reinforcement, RC-zoning, and tension stiffening formulations, plain concrete beams subjected to pure torsion are analysed. Two concrete beams, with square and rectangular cross-sections, respectively, are chosen[21]. The analysis input parameter is simply the mean cylinder compressive strength of the test series[21]. Tensile strength, Young's modulus, and tensile fracture energy are estimated from the cylinder strength by the JCI and CEB-FIP model code (1990) empirical formulas, respectively. Three different meshes are investigated. These are a coarse mesh representing the lower bound, a standard mesh as commonly employed in analysis, and a fine mesh requiring considerable computational resources.

The results for the rectangular section (specimen A2), as shown in **Fig.17,** indicate that even a coarse mesh gives close to acceptable predictions of cracking and ultimate torque (a value that is 15% too high). Only the descending branch gives divergent results. This is because computational failure is localised and located outside the twist reference length, and the unloading response of the material is mostly included in the reference zone specified in experiment due to the relatively large size of elements. Results with standard and fine meshes almost coincide until the peak and only slightly deviate in the descending part. For the square section (specimen A3), computed results are similar. Considering the spread of material parameters within the test series, the results are taken to be acceptable.

In **Fig.18,** the normalised ultimate torque for specimen A3 is plotted for the three different meshes. With the standard and finer meshes, the same ultimate torque is obtained, while the coarse mesh results in a slightly higher value since discretisation is too rough to follow the actual strain gradient.

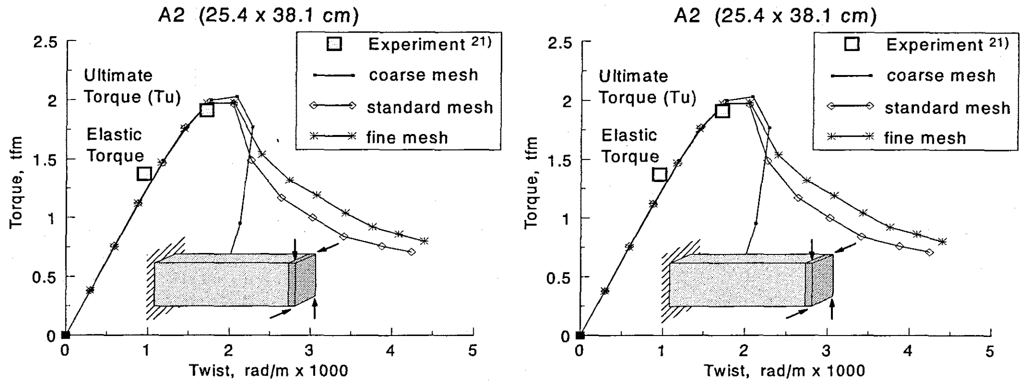


**Fig.17** Plain concrete rectangular (A2) and square (A3) section torsion beams: mesh size sensitivity study

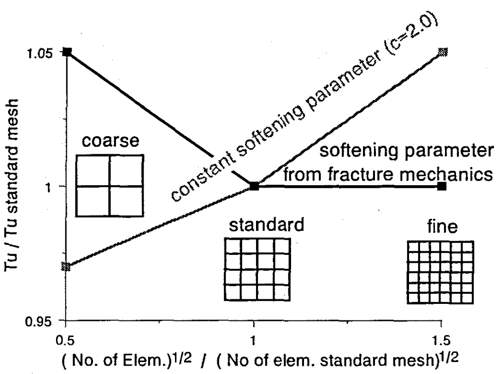


**Fig.18** Ultimate torque for mesh size-dependent and independent tension softening (specimen A3)

At the same time, specimen A3 is also analysed using mesh-independent tension softening, described by constant softening parameter c (c=2.0) in Eq.(3) [1]. Now, as the mesh gets more refined ultimate torque increases as expected.

However, it is interesting to note that for the standard mesh fracture mechanics approach[8] and experimentally obtained constant softening parameter[1] yield similar good results. Nevertheless, using the fracture mechanics approach the required objectivity with respect to mesh refinement seems to be obtained if too coarse a mesh is avoided.

## 4.2 Influence of RC zoning on torsion analysis

The efficiency of the 2D sub-space-based 3D-smeared crack model[4] and the mesh-independence of results have been demonstrated by analysing plain concrete beams subjected to torsional loading. Here, the concept of 3D RC zoning and anisotropic softening as well as mean yield strength (Chapter 3) are scrutinised by analysing RC members with full three-dimensional load bearing mechanisms, namely reinforced concrete torsion beams.

Mitchell and Collins[20] have tested several prestressed concrete beams under pure torsion load. Only one of these was a conventionally reinforced beam (P6), and this is chosen as the first target of analysis. Dimensions, material properties, and finite element discretization and load application are given in **Fig.19**. The results of the computed torque-twist relationships are compared with the experimental data[20] in **Fig.20**. When the RC zone is defined as only twice the concrete cover (2c), a large amount of energy is rapidly released just after initial cracking. Consequently, post-cracking stiffness and ultimate capacity are considerably reduced in comparison with experimental data.

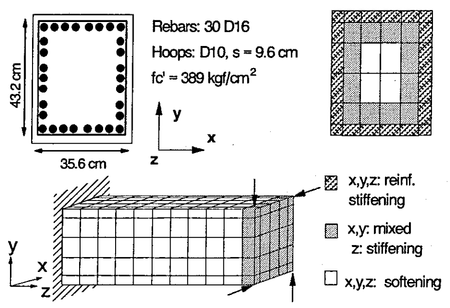


**Fig.19** Properties and RC-zoning of P6 torsion beam[20]

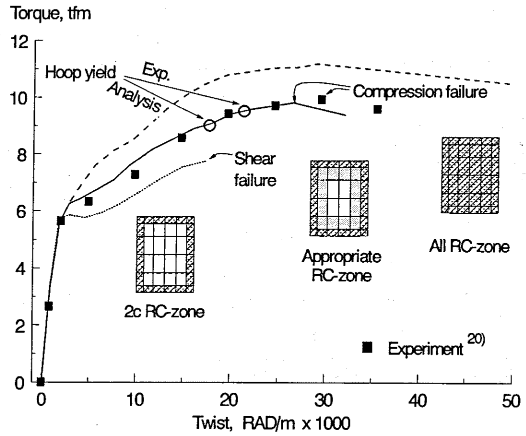


**Fig.20** Influence of RC-zoning on post-cracking torsion response (Specimen P6).

On the other hand, if the whole concrete volume is assumed to be reinforced concrete, the post-cracking stiffness and ultimate torque capacity are far too high. The RC volume determined according to the 3D zoning technique in chapter 3 (the proposed standard in this paper) leads to a reasonable torque-twist relationship. From this example, it is clear that neither the whole concrete volume nor a very small RC skin is appropriate for torsion analysis.

## 4.3 Influence of anisotropic yield strength

**Figure 21** shows hollow and solid section torsion members, designated by VH1 and VQ1.[17]. Reinforcement quantity is low such that yielding is anticipated as the primary failure mechanism. According to RC zoning and Eq.(12), an effective reinforcement ratio of about

0.4 % is obtained. With this value, the specimens are first analysed using average yield strength computed according to Eq.(13), independent of crack inclination. As depicted in **Fig.21**, premature yielding of the reinforcement occurs in this case. Next, $\rho_{eff}$ is directly computed from the observed crack spacing using Eq.(17) and the corresponding mean yield strength is again obtained by Eq.(13). The computed torque–twist relationship matches fairly well with the experimental data[17]. In particular, the yield moment and ultimate torque agree nicely (**Fig.21**). Finally, mean yield strength interpolation is employed as the proposed standard here for predicting structural response without the use of factor identification from the experimentally observed crack patterns. As with the first analysis, $\rho_{eff}$ is obtained from RC zoning and the corresponding mean yield strength for direct tension is computed from Eq.(13). Here, the resulting mean yield strength is reduced owing to the crack inclination relative to the reinforcing bars, as described by Eq.(14). The obtained results agree with those obtained from direct utilisation of crack spacing as well as the experimental data[19], as shown in **Fig.21**, explicitly supporting the validity of the interpolation approach.
Good agreement between numerically predicted and experimentally observed reinforcement yielding can also be found for specimen P6[20] (see **Fig.20**), further substantiating method. Thus, it may be concluded that the average yield strength of reinforcement does indeed depend on crack inclination relative to the steel bars, as proposed in this paper. Tension stiffening anisotropy and softening associated with steel orientation is crucial.

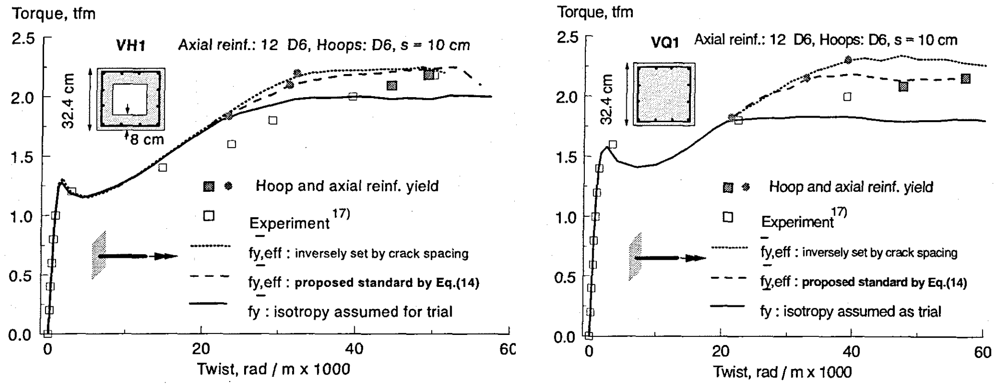


**Fig.21** Influence of anisotropic yield strength

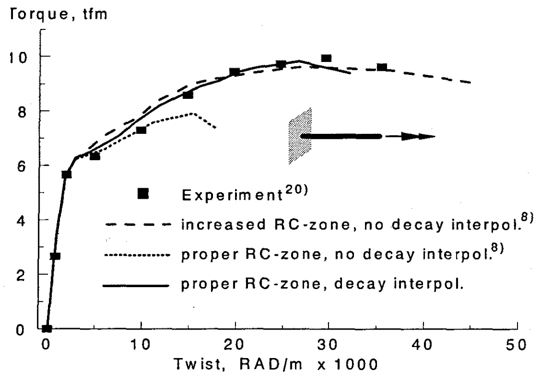


**Fig.22** Influence of shear decay onset and RC-zone: P6[20]

## 4.4 Effect of anisotropic shear transfer decay

Shear transfer decay, as introduced in chapter 3, may influence shear capacity or even failure mode as has been demonstrated for shear beams[8]. But, as pointed out previously, the shear strain level from which the decay of transferred shear stresses begins may also play an important role. In order to evaluate the effect of the proposed shear decay onset interpolation between that for cracks normal and parallel to the reinforcement, all other model parameters as previously introduced are kept constant in a further analysis. Computational results for specimen P6[19] are shown in **Fig.22**.

Since no decay onset interpolations are considered, meaning that shear decay starts at 4,000 μ for cracks normal to cracks in the RC zone and at 400 μ for all other crack inclinations with respect to the reinforcement, the analysis predicts premature failure. If the RC zone is increased beyond the size determined by the 3D RC-zoning method or if we adapt the standard proposed in this paper, the computational results closely approach the experimental data. Consequently, the authors tentatively accept the RC-zoning method in view of engineering applications. However, it is necessary to further discuss the possible combination of more refined RC zoning in terms of macro bond properties and shear decay in future.

## 4.5 Solid and hollow torsion members

For reinforced concrete members, it is well known that there is some variance in torsional response between thick-walled hollow members and solid ones, which otherwise have similar properties[20), 22]. To further solidify the analysis scheme for torsional RC members, four beams with solid (VQ-series) and hollow (VH-series) square cross sections were selected[17]. In all these beams, the axial and lateral reinforcement ratios coincide. Specimens VH2 and VQ4 are distinguished from specimens VH1 and VQ1 by 50% more reinforcement (**Fig.23**). All previously scrutinised methods of 3D RC zoning, anisotropic tension softening and interpolations, shear transfer decay, and anisotropic mean yield strength are considered in the analysis. The results of numerical simulation are compared with experimental data[17] in **Fig.23**. For 60$^{th}$ low and high reinforcement quantities, the ultimate torsional capacity of solid and hollow sections is, as anticipated, very similar. In specimens with low reinforcement content (VH1 and VQ1), numerical failure was by yielding of the reinforcement. The resulting large deformations finally caused concrete compression failure. Highly reinforced specimens (VH2 and VQ4), on the other hand, failed in diagonal concrete compression before reinforcement yielding. Similar failure mechanisms are also reported for the tested beams[17].

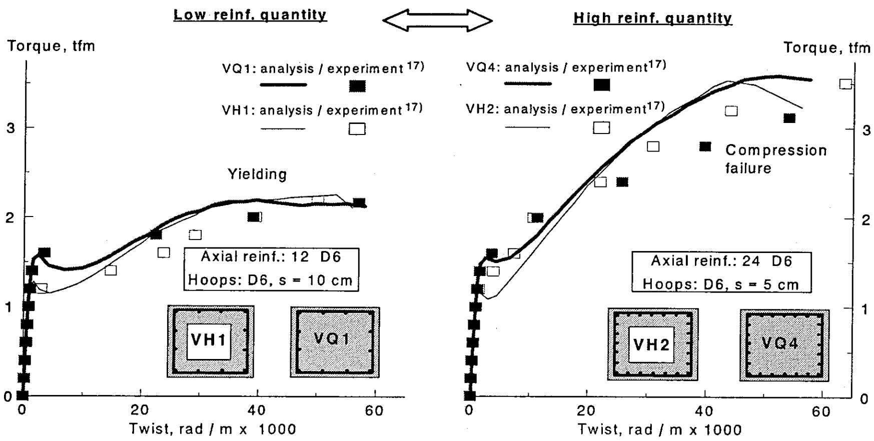


**Fig.23** Influence of anisotropic yield strength

## 5. RC COLUMNS SUBJECTED TO BI-AXIAL SHEAR

Studies of plain and reinforced concrete torsion members are useful for general verification of the 3Dsmeared crack model with unstable and stable propagation of 3D inclined cracks, respectively. However, it should be noted that even for inherently 3D torsion loading, the principal stress direction does not vary in 3D but rotates just in a restricted 2Dstress field. This means that the ability to simulate multi-directional cracks in full 3D has not been fully explored and verified by the analysis conducted so far. With this background in mind, short RC columns subjected to varying multi-directional shear forces are selected for scrutiny of the proposed schemes for 2D break down of the strain field and 3D re-composition of 2D partial stresses as well as the 3D anisotropy of tension fracturing and its interpolation, as described in section 3.

**Figure 24** illustrates the set-up of the short RC columns[23)] used for verification of the full 3D non-linear analysis frame. A constant axial load (150tf) and fixed horizontal load in the Y-direction (0, 15, 25, 35 tf for different specimens) are applied. After setting these forces, varying enforced displacements in the X-direction normal to the already applied shear are monotonically applied until failure (**Fig.24**). Under this load application scheme, there is considerable complexity in the stress fields accompanying tri-axially varying inclined cracks and corresponding principal stress directions. This means that spatial development of stress induced cracks is irregular, in contrast with reinforced concrete in 2D shear.

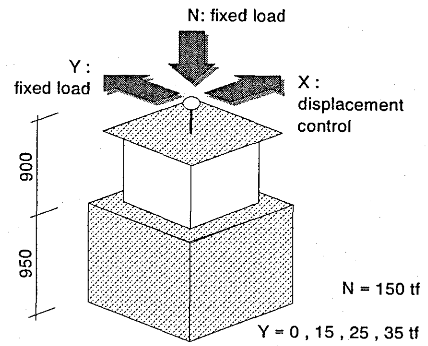


**Fig.24** Setup of short RC column loaded in

Specimens with two different reinforcement arrangements are tested[23)]. The S-series specimens include only three stirrups while specimens in the D-series have additional hoops in the X-direction (**Fig.25**). The reduced effectiveness of the additional hoops in D-series due to non-uniform stress distribution is taken into account by subtracting twice the minimum anchorage length (CEB-FIP MC-90) from the actual length and considering only this reduced length in the computation of premature bond stress development close to the concrete cover.

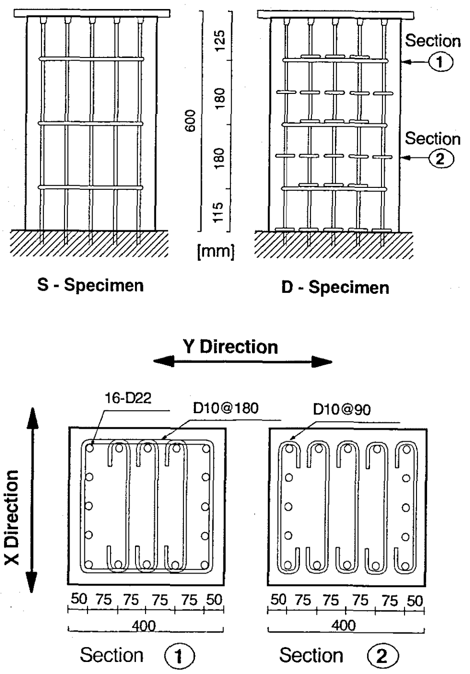


**Fig.25** Bi-axial shear reinforcement layout[23)]

### 5.1 Influence of anisotropic tension fracturing and interpolation

The concept of spatial variable tension softening/stiffening associated with crack direction relative to the steel reinforcement was discussed in section 3. It was concluded that cracked concrete should obey tension stiffening normal to the reinforcing bars and localised tension softening parallel to them.

This was referred to as anisotropic tension softening. The concept seems to be self-explanatory since it is physically evident that parallel cracks must soften and perpendicular ones stiffen (**Fig.26**), and hence element-wise isotropic tension stiffening is not versatile within the concept of spatial average-based modelling.

Nevertheless, utilising specimen D35 from D-series, as above described, the isotropic and anisotropic tension softening concepts are numerically compared. In all trial analyses, the horizontally applied constant force in the Y-direction is no longer sustained in computation, no matter how stably horizontal displacement is settled. Consequently, no plastic flow in the X-direction is shown in **Fig.26**. It is clear that isotropic tension stiffening can overestimate the actual load capacity. Only if all cracks form normal to the reinforcement can isotropic idealisation be expected to yield equivalent numerical results.

Anisotropic tension softening will be regarded as the standard from this point award. However, it remains necessary to scrutinise the influence of the interpolation method for arbitrally inclined cracks. It was previously argued that a direct interpolation of softening parameter *c*, which governs the slope of the descending branch of the tension stress-strain diagram as described in Eq.(3), would lead to a severe underestimation of the anticipated tension stiffening effect for cracks non- perpendicular to reinforcement, since it is non-proportional to the consumed fracture energy (**Fig.9**). Thus, the concept was introduced for solving the softening parameter for variable crack inclination from the interpolated normalised fracture energy $G_f*$, as illustrated in **Fig.9**.

Specimen D35 is chosen again for comparison of numerical results. It features the strongest directional shift between the initial and ultimate shear planes combined with uni-directional additional shear reinforcement making an accurate definition of tension softening/stiffening in crucial space. In **Fig.26**, numerical results for both the above-mentioned interpolation strategies are plotted. As expected, mere interpolation of softening parameter results in a load capacity much below the experimentally obtained value[23]. Interpolation of normalised fracture energy and the implicitly obtained corresponding softening factor, on the other hand, leads to fair agreement between analytical and experimental values of bi-axial shear capacity, and this is taken to be a verification of the proposed scheme of anisotropic tension fracture and fracture energy-based interpolations.

## 5.2 Bi-axial shear force interaction diagram

In order to further confirm that the proposed model is able to predict the evolution of the spatially inclined variable shear plane under non-proportional loading, all specimens in the above-described experimental series[23] are analysed. In **Fig.27**, the experimental and computed X-load versus X-displacement curves for all S- and D-series specimens are plotted. As the level of pre-imposed Y-load increases, the initial stiffness in the X-direction

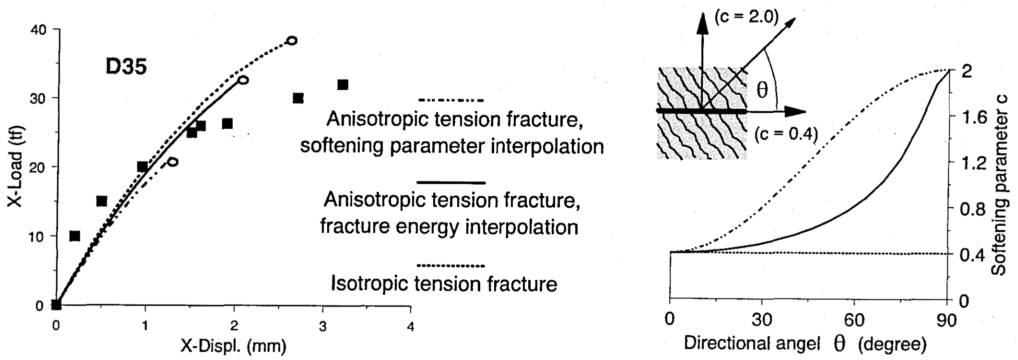


**Fig.26** Effect of isotropic or anisotropic tension fracture and interpolations

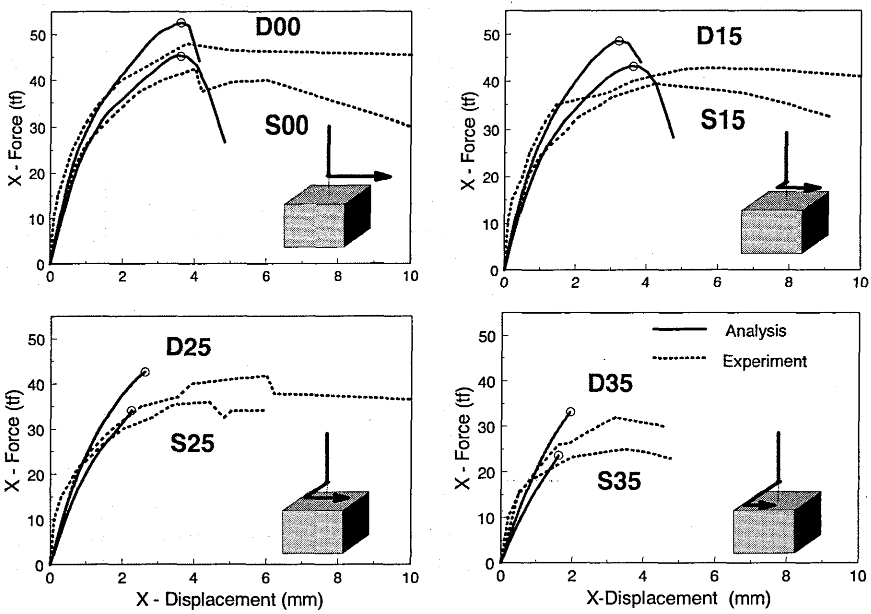


**Fig.27** Bi-axial shear : load-displacement diagram (X-direction)

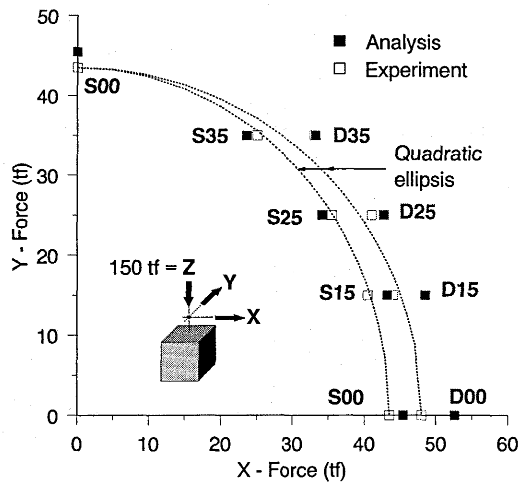


**Fig.28** Bi-axial shear : X-Y force interaction diagram

decreases in the computations due to pre-accumulated damage. The influence of additional hoops in the X-direction, improving stiffness and ultimate shear capacity in that direction, is qualitatively and correctly reflected in analysis.

**Figure 28** shows the shear force interaction diagrams. Failure mode in computations was judged by checking the instability of iterative calculations. Progressive cracking within finite elements and the accompanying energy release under enforced displacement are the criteria of shear failure. In cases where no post-peak response could be obtained, the numerical instability point was defined as the computed ultimate capacity and the instability was checked for absence of load steps influence. The analysis reflects the reduction in shear capacity in one direction as the shear load in the other direction increases. For the D-series specimen with additional X-reinforcement, shear capacity in the X-direction is improved. Here, the effect of the hoops seems to be overestimated in the simulation, even though only the reduced hoop length was considered in the computations, as noted above. Consequently, the predicted capacity in the X-direction is a little higher when there is lower shear force in the Y-direction.

As mentioned before (**Fig.24**), load application was mixture of force and displacement controlled loading. In force-controlled loading, no post-peak response is generally obtained. Then, looking at the computed load-displacement diagrams shown in **Fig.27**, it seems reasonable that for specimens with larger force-controlled pre-imposed Y-load (S25, S35, D25, D35) that remains at a constant level, no post-peak response could be computed. Since the constant Y-load largely contributes to the total force, no post-peak solution exists for numerical simulations with these perfect boundary conditions (**Fig.24**).

However, during the experiments[23)], once the ultimate load had been reached, the pre-imposed Y-load could not be kept constant but dropped swiftly. Only under such imperfect conditions, which different from the numerical simulations, does a post-peak response exist. On the other hand, for specimens with no or only a small force-controlled contribution to the total load (S00, S15, D00, D15), the descending branch could be computed with sustainable orthogonal shear force in Y-direction, though it is much steeper than that observed in experiments[23)].

Up to the peak of the load displacement diagrams, full 3D constitutive models work well with adequate accuracy for engineering purposes. The load interaction for multi-directional action can be well predicted in accordance with the experimental results. Nevertheless, in the descending portions of the diagrams, computation is not successful. In the experiments, significant residual post-peak strength and ductility are observed[23)]. In fact, the arc-length method of iteration with some restraint cannot be adopted due to the almost-constant horizontal load. Here, strain localisation in compression remains unsolved in the finite element analysis. Post-peak compression softening can be regarded as one of the essential requirements for a sound prediction of the descending part of the load-deflection diagram. Furthermore, it should be noted that the present formulation does not explicitly consider any dowel action of the reinforcing bars, which might become important as an element of resistance in localised shear cracks close to or post-peak.

### 5.3 Bi-directional displacement path

In evaluating the numerical simulation results it is not sufficient only to compare the bi-axial shear force diagram with experimental data. As a further verification, the displacement path of bi-directional loaded short columns is studied. In **Fig.29**, the bi-directional displacement history is plotted. Displacement at the ultimate shear capacity is marked by ° for the numerical values and by • for the experimental data[23)]. Any further displacement is that of the post-peak descending branch. In comparing analytical results with experimental data, the effect of reinforcing bar pullout from footing needs to be considered[1),24)]. And because the experimental data [23)] includes only the total response, with no separate member and joint-based displacements, joint behaviour needs to be taken into account in the analysis[1)].

First, the analytical displacement path on a member basis is already shown in **Fig.27**. In the following, joint-based displacement is determined in a separate analysis employing the RC discrete crack model[25,26)] for the column-footing joint together with rigid brick elements for the columns. The joint element models the pullout of reinforcing steel from concrete and the mechanism of stress transfer due to aggregate interactions along the crack surface[25)]. Dowel action of the reinforcing steel is neglected.

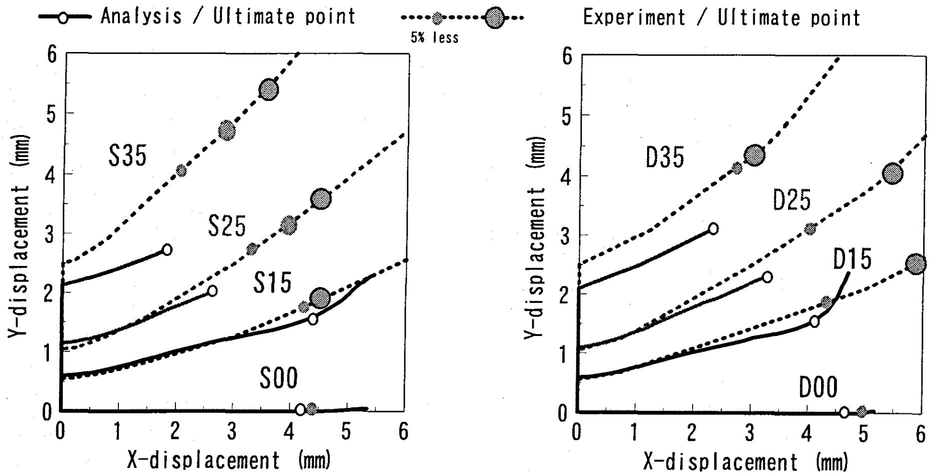


a) S-series b) D-Series

**Fig.29** Bi-axial displacement path: member + joint response in analysis

**Figure 29** is a superposition of the computed joint and member displacements with the experimental data[23]. The general trend of the experimental data seems to be reproduced by this analysis, especially the flow direction of column heads under multi-directional action. Nevertheless, it must be admitted that some quantitative discrepancy remains. One reason for this could be that the shear transfer model[13] used in the joint element [25] is one developed for 2D problems. Applied to 3D analysis in the X- and Y-directions, shear transfer is not interrelated but assumed independent. This could partly explain the larger gap between the experimental and analytical displacement paths for specimens with strong bi-directional loading (S25, S35, D25, D35).

Further, attention must be paid to the time-dependent flow of displacement when the force is kept constant at a level close to capacity in experiment. This was experienced in the experiment, but the analysis with time-independent RC modelling does not cover rapid inelastic creep flow.

## 5.4 Visualisation of varying crack inclination

A full 3D analysis of concrete structures results in a huge amount of output data giving displacement and reaction force for each nodal point as well as complete average stress and strain vectors and internal parameters of plasticity, damage, and cracking at each Gaussian integration point. In employing a quadratic interpolation function and 2$^{nd}$ order integration, we have information for 20 nodes and eight integration points for each finite brick element. Handling such an abundance of information in a thoughtful way could provide researchers with many valuable insights into the numerical, and presumably the real behaviour of complex concrete structures.

Post-processing for 2D computer codes is well advanced and many nice graphical tools are available to make the daily life of concrete researchers and engineers easier. However, there is a shortage of analysis tools of full 3D and, naturally, post-processing codes for 3D data are even less developed. Nevertheless, especially for the understanding of varying 3D inclined crack planes as observed in multi-directional loading of reinforced concrete, such visualisation is essential. The advent of multi-media technology now presents new opportunities for quick advances. Using the Virtual Reality Modelling Language, Takahashi and Maekawa[27] provide a new opportunity for "looking inside" cracked concrete. Node and

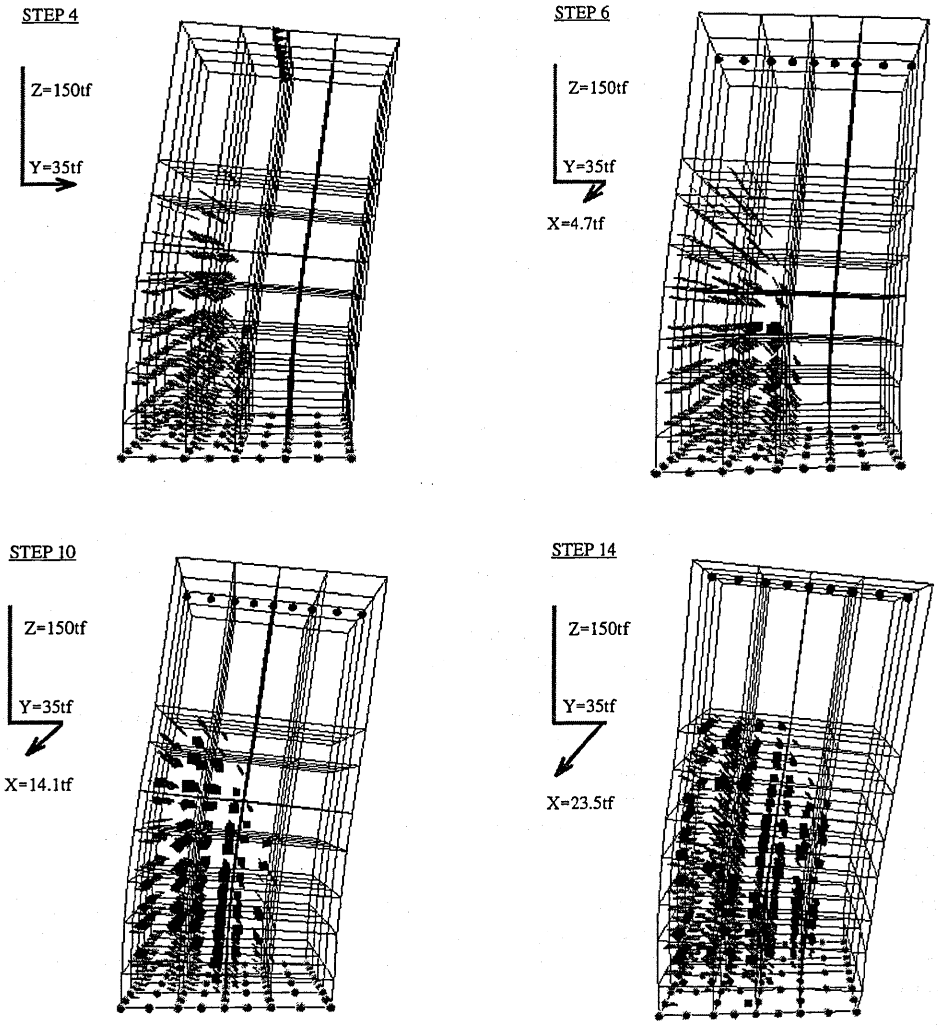


**Fig.30** Evolution of 3D inclined variable cracks under multi-directional non-proportional loading: 35

integration point data are read and transformed into a VRML input format. Particular care is taken of the spatial orientation of the predominant crack at each integration point[27]. As non-proportional loading changes in direction, new cracks are introduced and came to govern in place of the existing crack, so the visualised crack direction changes. Deformation data are also collected. In this way, a graphical tool has been constructed that makes it possible to observe the complex cracking behaviour of multi-directionally loaded reinforced concrete[27].

As an example, the step-by-step development of predominant three-dimensionally variably inclined cracks for specimen S35 is given here. Specimen S35 is selected because it guarantees the maximum directional variation of the initial shear cracking plane and intersection of the final shear failure plane. A relatively large Y-force of 35tf is first applied, followed by displacement-controlled loading up to failure in the perpendicular X-direction as seen in **Fig.30**. The crack plane at each Gaussian integration point is indicated by a small plate with a spatial orientation determined according to the observed predominant crack. Deformation of the specimen is shown as well.

In step 1, an axial load of 150tf is applied and naturally no cracks are found for the load is compressive and far from ultimate. In steps 2 to 4, the fixed horizontal Y-force is applied in 11.67tf increments, resulting in a total of 35 tf. Once the full Y-force is applied in step 4 (**Fig.30**), typical inclined shear cracks have developed. As the Y-direction is kept clamped and displacement-controlled loading is applied in the perpendicular X-direction from step 5 on, the initially induced cracks remain predominant until step 6 (**Fig.30**) and only few cracks change orientation through the generation of new non-orthogonal cracking. By step 10 (**Fig.30**), most of the plates representing the governing crack planes of each integration point have already turned from the initial Y-plane inclination toward spatial inclination. This tendency is reinforced in the following steps, resulting in final shear failure taking place in a completely different plane from the originally induced shear crack plane. Step 14 (**Fig.30**) is ultimately identified as the step just before unstable crack propagation occurs and, hence, is designated as the ultimate load level. Here, the fully three-dimensionally inclined shear plane can be clearly identified.

## 6. CONCLUSIONS

Full three-dimensional constitutive laws for reinforced concrete have been proposed for RC solids with multi-directional cracks, and their applicability under monotonic forces was examined. A complete 3D-space expanded EPF model[2), 3)] was proposed for un-cracked concrete. For 3D cracked concrete, a 2D breakdown and 3D re-composition scheme of smeared crack analysis[4)] was scrutinised. The mesh-independence of the formulation was demonstrated by analysing plain concrete torsion beams with different mesh discretizations. Anisotropy of tension fracturing was recognised as bond mechanism is stably controlled, and dispersed crack propagation for cracks normal to the reinforcement must be distinguished from unstable, localised behaviour of cracks parallel to the reinforcement.

To account for the anisotropy of tension fracturing in the 3D domain, a method of three-dimensional RC zoning and fracture energy-based softening parameter interpolation was presented. In a similar way, it was concluded that the average-based response of tension reinforcement depends on the crack inclination relative to the reinforcement. Where cracks parallel to reinforcement may result in behaviour close that of an unconstrained bare bar, normal cracks results in localised plasticity in the vicinity of those cracks. Crack inclination-dependent interpolation of average yield strength was found an effective measure to address this phenomenon.

The proposed framework of 3D nonlinear analysis was successfully applied to the numerical response prediction of hollow and solid torsion members with low and high reinforcement rations. For short RC columns under multi-axial loading, the 3D inclined variable shear plane and its associated shear failure were simulated.

Further development toward a truly versatile computational tool for examining the structural performance of reinforced concrete under complex loading patterns is a challenging topic of research. The performance-based design schemes that future structural codes will demand mean that engineers must check for specified limit states. Here, especially, structures have to be checked for seismic or accidental loading in reasonable consistency with material and structural mechanics. The physically consistent solutions of the compression localisation and buckling of reinforcement embedded in concrete are regarded as crucial areas of further research toward obtaining a reliable post-peak response.

**REFERNCES**


1) Okamura, H., and Maekawa, K.: *Nonlinear analysis and constitutive models of reinforced concrete*, Gihodo- Shuppan Co., Tokyo, 1991.
2) Maekawa, K., Takemura, J., Irawan, P., and Irie, M.: Triaxial elasto-plastic and continuum fracture model for concrete," *Concrete Library*, JSCE, No. 22, pp.131-161, 1993.
3) Hauke, B., and Maekawa, K.: Three-dimensional reinforced concrete model with multi-directional cracking, *Computational modelling of concrete structures*, de Borst et al. eds., Balkema, Rotterdam and Brookfield, pp. 93-102, 1998.
4) Maekawa, K., Irawan, P., and Okamura, H.: Path-dependent three-dimensional constitutive laws of reinforced concrete – formulation and experimental verifications, *Structural Engineering and Mechanics*, Vol. 5. No. 6, pp. 743-743, 1997.
5) Fukuura, N., and Maekawa, K.: Multi-directional crack model for in-plane reinforced concrete under reversed cyclic actions – 4 way fixed crack formulation and verification, *Computational modelling of concrete structures*, de Borst et al. eds., Balkema, Rotterdam and Brookfield, pp. 143-152, 1998.
6) Cervenka, V., and Margoldova, J.: Tension stiffening effect in smeared crack model, *ASCE EMD Specialty Conference*, May 21-23, University of Colorado, Boulder, USA, 1995.
7) Shima, H., Chou, L., and Okamura, H.: Micro and macro models for bond behaviour in reinforced concrete, *Journal of the Faculty of Engineering, The University of Tokyo (B)*, Vol. IIIXIX, No. 2, pp. 133-194, 1987.
8) An, X., Maekawa, K., and Okamura, H.: Numerical simulation of size effect in shear strength of RC beams, *J. of Materials, Concrete Structures and Pavements*, JSCE, Vol. 35, pp. 297-316, 1997.
9) Gupta, S., and Tanabe, T.: Unified concrete plasticity model in three dimensional analysis of reinforced concrete members, *Proc. of JCI*, pp. 561-566, 1997.
10) Barzegar, F., and Maddipudi, S.: Three-dimensional modelling of concrete structures, *J. of Struct. Eng*, Vol. 123, pp. 1339-1356, 1997.
11) Salem, H.M., Hauke, B., and Maekawa, K.: Fracture of concrete cover – its effect on tension stiffening and modeling, *Proc. of JSCE annual convention*, 1998.
12) Bazant, Z.P., and Oh, B.: Crack band theory for fracture of concrete, *RILEM Mat. Struct.*, Vol. 16, pp.155-177, 1983.
13) Li, B., Maekawa, K., and Okamura, H.: Contact density model for stress transfer across cracks in concrete, *Journal of the Faculty of Engineering, The University of Tokyo (B)*, Vol. XL, No. 1, pp. 9-52, 1989.
14) Bujadham, B., and Maekawa, K.: The universal model for stress transfer across cracks in concrete, *Proc. of JSCE*, No. 451/V-17, pp. 277-287, 1992.
15) General Task Group 22 of the CEB: *RC elements under cyclic loading*, CEB state of the art report, Thomas Telford, London, 1996.
16) Salem, H.M., and Maekawa, K.: A versatile computational model for reinforced concrete in tension, *Proc. of annual meeting JSCE Kanto,* 1998.
17) Leonhardt, F., and Schelling, G.: *Torsionsversuche an Stahlbetonbalken,* DAfStB, Ernst & Sohn, Berlin, 1974.
18) Salem, H.M.: *Enhanced tension stiffening model and application to nonlinear dynamic analysis of reinforced concrete*, Ph.D thesis, The University of Tokyo, 1998.
19) Hsu, T.T.C.: Torsion of structural concrete – a summary on pure torsion, *Torsion of structural concrete*, SP-18, ACI, Detroit, pp. 165-178, 1968.
20) Mitchell, D., and Collins, M.P.: Influence of prestressing on torsional response of concrete beams, *PCI Journal*, Vol. 23, No. 3, pp. 55-72, 1978.
21) Hsu, T.T.C.: Torsion of structural concrete – plain concrete rectangular sections, *Torsion of structural concrete*, SP-18, ACI, Detroit, pp. 203-238, 1968.
22) Hsu, T.T.C.: Torsion of structural concrete – behaviour of reinforced concrete rectangular members, *Torsion of structural concrete*, SP-18, ACI, Detroit, pp. 261-306, 1968.

23) Yoshimura, M.: Failure envelope of RC columns in two-way shear, *Summaries of Technical Papers of Annual Meeting*, AIJ, pp. 199-200, 1996 (in Japanese).
24) Mishima, T., and Maekawa, K.: Development of RC discrete crack model under reversed cyclic loads and verification of its applicable range, *Concrete Library*, JSCE, No. 20, pp115-142, 1992.
25) Maekawa, K., and Qureshi, J.: Behavior of embedded bars in concrete under combined axial pullout and transverse displacement, *Concrete Library*, JSCE, No. 28, 1992.
26) Hauke, B.: *Three-dimensional modelling and analysis of reinforced concrete and concrete composites*, PhD thesis, The University of Tokyo, 1998.
27) Takahashi, T., and Maekawa, K.: Visualisation of three dimensional RC crack analysis using immersive multi-screen display, *Proc.of JCI,* Vol 20, No. 1, pp. 149-154, 1998 (in Japanese).